optics

MDPI

Article

A Concept and Numerical Study of Refractive-Index-Based pH Estimation Using an Etched Addressed Fiber Bragg Structure with Microwave Photonic Interrogation

Alaa N. D. Alhussein *, Aliya A. Kamaleeva, Bulat I. Valeev, Timur A. Agliullin, Artem A. Kuznetsov and Airat Zh. Sakhabutdinov *

Department of Radiophotonics and Microwave Technologies, Kazan National Research Technical University Named After A. N. Tupolev—KAI, K. Marx St. 10, Kazan 420111, Russia; aakamaleeva@kai.ru (A.A.K.); bivaleev@kai.ru (B.I.V.); taagliullin@kai.ru (T.A.A.); aakuznetsov@kai.ru (A.A.K.)

* Correspondence: alaanajeed8181@gmail.com (A.N.D.A.); azhsakhabutdinov@kai.ru (A.Z.S.)

Abstract

This study investigates the feasibility of using an etched addressed fiber Bragg structure (EAFBS) as the sensing element in a microwave-photonic system for local pH monitoring. A theoretical model is developed that incorporates transmission-spectrum analysis of the addressed Bragg structure and evaluation of the effective refractive index of the guided mode as a function of the surrounding medium parameters. The model establishes a relationship between the refractive index of the surrounding medium and the spectral response of the EAFBS. Using the proposed mathematical model, numerical simulations are performed for three pH ranges corresponding to various liquid media. The results of numerical studies show that in all in the pH ranges, the address frequency varies nearly linearly, with a sensitivity of approximately 1.66 GHz/pH (pH range of 4–7), 2.64 GHz/pH (pH range of 7–10), and 1.92 GHz/pH (pH range of 10–13), whereas its temperature dependence in the range of 35–45 °C is approximately 1.06 GHz/°C. These results indicate that the proposed EAFBS-based approach can provide a foundation for high-speed pH sensing systems with a simplified interrogation scheme and potential capability for frequency-division multiplexing.

Keywords: microwave-photonic interrogation; pH sensing; addressed fiber Bragg structure; etched fiber Bragg grating; refractive index sensing; fiber-optic sensor; numerical study

Check for updates

Academic Editor: Davide Rocco

Received: 28 May 2026

Revised: 1 July 2026

Accepted: 3 July 2026

Published: 6 July 2026

1. Introduction

Monitoring hydrogen ion concentration (pH) is one of the fundamental tasks in analytical, environmental, biomedical, and industrial measurements, since pH directly affects the course of chemical and biological processes, the stability of media, and the reliability of process control [1,2]. Accurate pH measurement is critically important for chemical analysis, environmental monitoring, and medical diagnostics [3] and remains essential for both scientific research and practical applications [4–6]. Accordingly, there is sustained interest in the development of sensing systems that provide not only adequate measurement accuracy, but also high noise immunity, the capability for local and continuous monitoring, and applicability in chemically aggressive and complex media [7,8].

Among the available solutions, fiber-optic pH sensors occupy a prominent position. Previous studies have shown that fluorescence-based [9–11], absorption-based [12–14],

 https://doi.org/10.3390/opt7040047

plasmonic [15–17], interferometric [18–20], Bragg-grating-based [21–23], luminescence-based [24,25], and evanescent-wave-based [26] fiber-optic approaches have all been employed for pH monitoring. This diversity confirms the considerable potential of photonic methods for pH sensing and indicates that fiber-optic sensors constitute one of the most promising classes of sensing elements for modern pH measurement systems [27–29].

At the same time, the practical deployment of fiber-optic pH sensing systems remains limited by the complexity and cost of their interrogation units. A substantial proportion of the reported approaches requires spectral analyzers, whereas improved measurement accuracy generally demands higher spectral resolution of the interrogation system [30–35]. This significantly increases the overall system cost and reduces the attractiveness of such solutions for multisensor and application-oriented implementations. Therefore, one of the key limitations of the existing fiber-optic pH sensing systems is associated not so much with the sensing element itself as with the architecture used to acquire and process its spectral response.

To better position the proposed EAFBS sensor within the current state of the art, Table 1 summarizes representative fiber-optic pH sensors reported in the literature, highlighting their sensitivity, operating range, temperature-related characteristics, interrogation methods, and validation status. The comparison illustrates the diversity of sensing mechanisms and interrogation approaches currently employed for fiber-optic pH monitoring.

Table 1. Quantitative comparison of representative fiber-optic pH sensors and the proposed microwave-photonic EAFBS sensor.

Sensor Type	pH Range	Sensitivity	Temperature Cross-Sensitivity	Interrogation Method	Validation	Ref.
Sodium-alginate-coated microfiber Bragg grating (µFBG)	4–12	−265 pm/pH (higher-order mode)	9.5–9.6 pm/°C (dual-resonance compensation)	Wavelength-shift tracking	Experimental	[21]
PAA/PAH polymer waveguide Bragg grating	4–7	10.4 nm/pH	Not reported	Bragg wavelength shift	Numerical simulation	[22]
Cavity-enhanced lab-on-fiber optrode	2.9–8.0	Up to 315 nm/pH	Thermal control required during measurements	Fabry–Perot cavity spectral interrogation	Experimental	[32]
PANI-coated tapered optical fiber/D-shaped POF	2–9	−0.22 dB/pH (tapered fiber)	Negligible temperature cross-sensitivity	Intensity-based optical interrogation	Experimental	[33]
BY/PAH-coated uncladded optical fiber	6.6–9.4	21–23 nm/pH	Not reported	Absorbance peak wavelength tracking	Experimental	[34]
GO/PVA-coated π-phase-shifted LPFG	4.0–9.2	−1.0166 nm/pH	Simultaneous temperature compensation (0.2128 nm/°C)	Multi-peak wavelength interrogation	Experimental	[35]
Partially etched addressed fiber Bragg structure (EAFBS)	4–7	1.66 GHz/pH	1.06 GHz/°C	Microwave-photonic address-frequency interrogation	Numerical simulation	This work
	7–10	2.64 GHz/pH				
	10–13	1.92 GHz/pH				

As shown in Table 1, most reported fiber-optic pH sensors rely on wavelength- or intensity-based interrogation schemes and often require spectral analysis equipment. While several approaches demonstrate high pH sensitivity, their practical deployment may be constrained by interrogation complexity, temperature-related effects, or limited compatibility with multiplexed sensing architectures. These limitations motivate the development of alternative interrogation strategies capable of preserving sensing performance while reducing system complexity. Recent microwave-photonic interrogation schemes based on optical interferometers have demonstrated high sensitivity and tunable dynamic range for FBG sensing applications [36].

A promising direction in this context is the transition to addressed and microwave-photonic interrogation principles. Recent studies have demonstrated that microwave-photonic interrogation can provide improved signal-to-noise ratio, enhanced sensitivity, and efficient electrical-domain processing for fiber-optic sensing systems [37]. Within this approach, processing of the sensor response is shifted from the optical domain to the microwave-frequency domain, where the signal can be extracted and analyzed via the beat-signal envelope at the address frequencies in the low-noise operating region of the photodetector. Importantly, in addressed fiber Bragg structures (AFBS), the address frequency is not an externally imposed signal feature, but an intrinsic property of the sensing element itself. This makes it possible to develop sensing systems that combine high sensitivity, increased interrogation speed, and simplified optoelectronic implementation [38–42]. Additional opportunities arise from the use of hybrid sensor architectures [43–45].

Recent microwave-photonic approaches have also demonstrated sensitivity enhancement through interferometric and Vernier-effect-based interrogation of FBG sensors, including point-wise and quasi-distributed sensing architectures [46].

Within this framework, particular interest is associated with modified addressed fiber Bragg structures derived from conventional AFBSs with two discrete symmetric phase shifts, which are suitable for microwave-photonic interrogation [38]. At the same time, it is necessary to ensure that the spectral response remains sensitive to variations in the refractive index of the surrounding medium. This can be achieved by enhancing the interaction of the evanescent field with the surrounding medium through a reduction in the cladding diameter (fiber etching) [47,48].

In the proposed configuration, only one section of the addressed fiber Bragg structure is subjected to selective chemical etching, while the remaining sections preserve the original fiber geometry. The etched section serves as the sensing region, where enhanced interaction between the evanescent field and the surrounding medium increases the refractive-index sensitivity of the structure. Throughout this paper, the term etched addressed fiber Bragg structure (EAFBS) refers to an addressed fiber Bragg structure incorporating such a locally etched sensing section.

The aim of this study is to provide a theoretical justification for a sensor architecture based on the etched addressed fiber Bragg structure (EAFBS) for local pH monitoring and to analyze the physical and system-level conditions under which pH-induced variations can be reliably mapped onto changes in the signal parameters under microwave-photonic interrogation. The study focuses on establishing the relationship between the refractive index of the surrounding medium, the spectral response of the EAFBS, and its address frequency, as well as on a qualitative assessment of the extent to which this approach can improve the performance-to-complexity ratio of fiber-optic pH sensing systems.

The novelty of the proposed approach lies in combining the local refractometric sensitivity of an etched fiber section with an addressed spectral response suitable for microwave-photonic interrogation. A preliminary concept of pH sensing based on etched addressed fiber Bragg structures was presented in the previous work [49], where the feasibility of enhancing refractive-index sensitivity through fiber etching and the applicability of EAFBS sensors for pH monitoring in the pH range 11.0–13.7 were demonstrated. In contrast, the present study develops a microwave-photonic interrogation framework and establishes a quantitative relationship between pH-induced refractive-index variations, the EAFBS transmission spectrum, and the address frequency. In addition, the study considers three pH ranges with various model calibration coefficients to demonstrate the applicability of the proposed sensing element for various media under study. Particular attention is given to the use of the address frequency as the primary measurement parameter, as well as to the analysis of frequency and amplitude responses and temperature cross-sensitivity within the proposed interrogation architecture.

2. Sensor Architecture and Microwave-Photonic Interrogation Principle

The sensor design is based on a modification of an addressed fiber Bragg structure with two π-phase shifts [50], with the key difference that the outer cladding of one of the uniform sections is partially or completely removed. This creates a localized region in which the surrounding medium interacts directly with the evanescent field (Figure 1). As a result, the sensing element retains the addressed nature of its spectral response while simultaneously acquiring sensitivity to the refractive index of the surrounding medium.

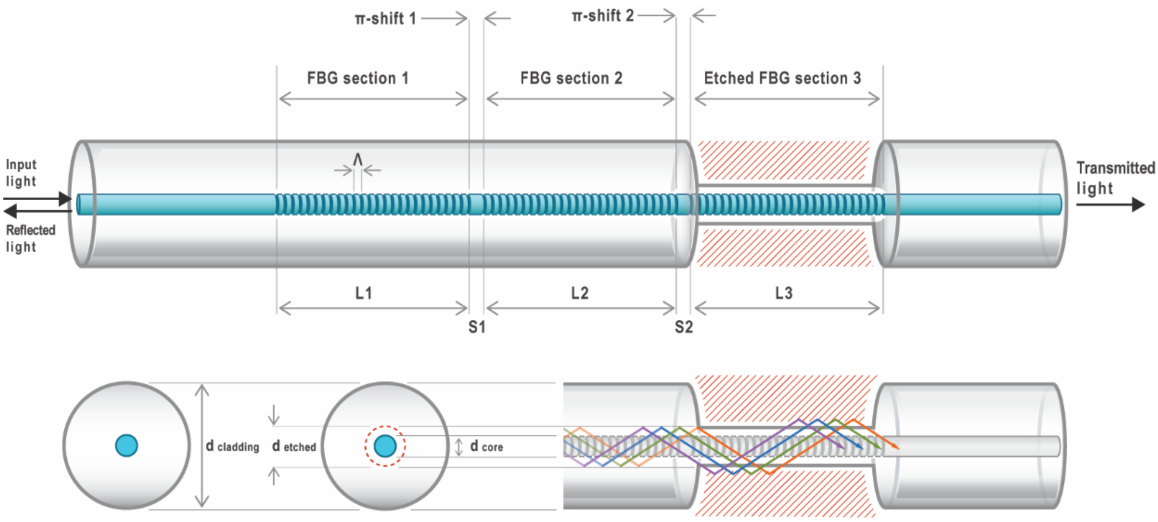

Figure 1. Scheme of the proposed EAFBS used as the sensing element, where only the third grating section is selectively etched.

From a fabrication perspective, the proposed structure can be realized by first inscribing the addressed fiber Bragg structure and subsequently performing selective chemical etching of the third grating section while protecting the remaining regions of the fiber. In this way, only the designated sensing region is exposed to the etching process, whereas the other sections preserve the original fiber geometry. The detailed optimization of fabrication parameters is beyond the scope of the present theoretical study.

The operating principle of the EAFBS is based on variations in the effective refractive index of the guided mode within the etched section. Reducing the cladding thickness increases the fraction of the optical field interacting with the surrounding medium; therefore, changes in its refractive index lead to a modification of the modal conditions and, consequently, to a shift in the spectral response of the EAFBS. Figure 2 shows an illustrative transmission spectrum of the EAFBS together with the optical bandpass filter profile used to select the addressed spectral components.

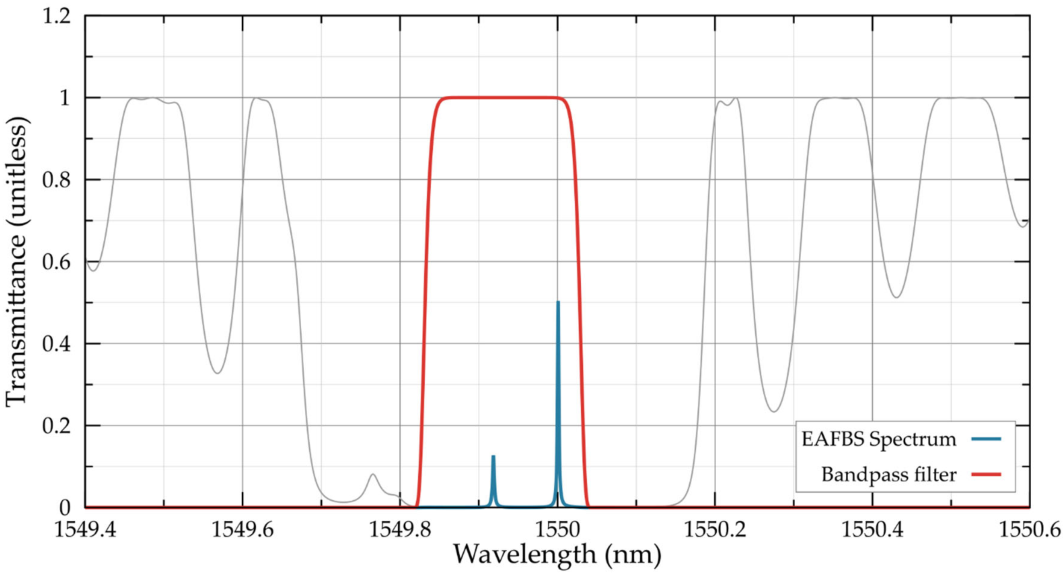

Figure 2. Illustrative transmission spectra of the EAFBS (blue curve) with optical bandpass filter profile (red curve).

Therefore, the proposed EAFBS operates fundamentally as a refractive-index sensor, while pH measurement is achieved indirectly through the dependence of the surrounding medium's refractive index on pH.

In the proposed architecture, the primary measured output is the address frequency, whereas the refractive index of the surrounding medium serves as the intermediate physical quantity linking the external chemical state to the sensor response. The measurement principle can be described as follows: a change in the pH of the surrounding medium leads to a change in its refractive index, which, through interaction via the evanescent field, modifies the effective refractive index of the etched fiber section for the guided mode. This, in turn, results in a shift in the spectral response of the EAFBS, specifically altering its address frequency, which is detected using microwave-photonic interrogation techniques. The conversion from refractive index to pH is performed through a calibration relationship specific to a given class of solutions.

The microwave-photonic interrogation principle is based on transferring the response from the optical domain to the microwave-frequency domain, as illustrated in Figure 3.

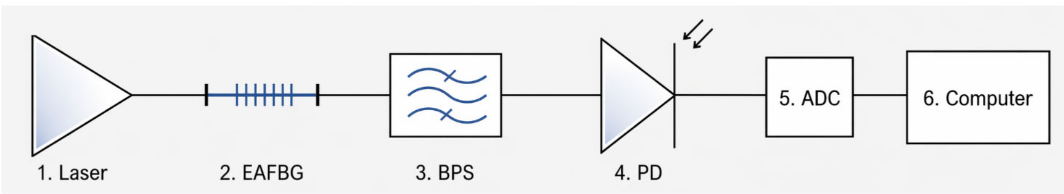

Figure 3. Sensor interrogation scheme.

Radiation from a broadband laser source (Laser—1) is directed to the EAFBS (2). From the full transmission spectrum, only the portion containing two high-Q spectral components that form the addressed feature is selected using an optical bandpass filter (BPF—3). The filtered signal is then detected by a photodetector (PD—4), digitized (ADC—5), and sent to the processing unit (Computer—6). The microwave-photonic interrogation scheme does not require complex or expensive components, which significantly reduces the demands on the interrogation system compared with full spectral analysis, increases the interrogation speed, and enables multisensor configurations with frequency-division multiplexing.

3. Theoretical Background

3.1. Transmission-Spectrum Model of the EAFBS

The theoretical model of the sensor is based on representing the fiber Bragg grating as a multilayer periodic structure with a spatially varying refractive index, for which the reflection and transmission spectra are calculated using the transfer matrix method. The transfer matrix of each uniform section of the EAFBS is expressed as a function of the optical wavelength (λ), grating length (L), effective refractive index (n_{eff}), grating period (Λ), and induced refractive index modulation (Δn). Accordingly, the spectral response is obtained by sweeping the wavelength and evaluating the corresponding reflection and transmission coefficients:

$$\mathbf{T}_{\mathrm{FBG}} = \begin{bmatrix} \cosh(\gamma L) - j\frac{\Delta\beta}{\gamma}\sinh(\gamma L) & -j\frac{\kappa}{\gamma}\sinh(\gamma L) \\ j\frac{\kappa}{\gamma}\sinh(\gamma L) & \cosh(\gamma L) + j\frac{\Delta\beta}{\gamma}\sinh(\gamma L) \end{bmatrix}, \tag{1}$$

κ, Δβ, and γ are defined as:

$$\kappa = \pi\frac{\Delta n}{\lambda},\ \ \Delta\beta = \frac{\pi}{\Lambda} - 2\pi\frac{n_{\mathrm{eff}}}{\lambda},\ \ \gamma = \sqrt{|\kappa|^2 - \Delta\beta^2}\ , \tag{2}$$

In this work, the EAFBS is modeled as a quasi-periodic structure whose spectrum is formed by three identical, sequentially arranged homogeneous FBG sections separated by uniform fiber segments. The lengths of these segments (S) are chosen to be odd multiples of half the grating period, i.e., ($S = \Lambda\cdot(2k + 1)$, $k \in \mathbb{Z}$). The transfer-matrix formalism is applied to all uniform sections of the structure. However, only the third section is subjected to cladding etching and interacts directly with the surrounding medium, whereas the first and second sections preserve the original fiber geometry. Consequently, the effective refractive indices of the first and second sections remain unchanged, while the effective refractive index of the third section depends on the refractive index of the surrounding medium and is responsible for the sensing response of the EAFBS. The transfer matrix of a uniform fiber segment is expressed as a function of its length (S), the optical wavelength (λ), and the permittivity (ε) and permeability (μ) of the optical fiber medium:

$$\mathbf{T}_{\mathrm{M}}(\lambda, \varepsilon, \mu, S) = \begin{bmatrix} e^{-j\cdot L\cdot\gamma} & 0 \\ 0 & e^{j\cdot L\cdot\gamma} \end{bmatrix}\ , \tag{3}$$

where

$$\gamma = \frac{\pi}{\lambda}\sqrt{2\mathrm{Re}\varepsilon\cdot\mathrm{Re}\mu}\left(\sqrt{\sqrt{1-\left(\frac{\mathrm{Im}\varepsilon}{\mathrm{Re}\varepsilon}\right)^2}+1} - j\sqrt{\sqrt{1-\left(\frac{\mathrm{Im}\varepsilon}{\mathrm{Re}\varepsilon}\right)^2}-1}\right)\ . \tag{4}$$

The transfer matrix of the EAFBS is expressed as the product of the transfer matrices of the three homogeneous FBG segments and the two intermediate uniform fiber sections between them:

$$\mathbf{T}_{2\pi\text{-FBG}}\ (\lambda, L_{\mathrm{FBG}}, n_{\mathrm{eff}}, \Lambda, \Delta n, S, n_0) = \mathbf{T}_{\mathrm{FBG}} \times \mathbf{T}_{\mathrm{M}} \times \mathbf{T}_{\mathrm{FBG}} \times \mathbf{T}_{\mathrm{M}} \times \mathbf{T}_{\mathrm{FBG}}\ . \tag{5}$$

A variation in the effective refractive index of the etched section modifies the overall transfer matrix and, consequently, shifts the transmission spectrum. This formulation enables the external perturbation applied to a localized region of the structure to be directly related to changes in the overall spectral response of the sensor.

https://doi.org/10.3390/opt7040047

3.2. Analysis of the Etched Section

The effective refractive index of a homogeneous FBG segment with an etched cladding is a function of the refractive indices of the core, the residual cladding, and the surrounding medium, as well as the geometry of the fiber cross-section. Considering that, in standard telecommunication fibers, the refractive indices of the core and cladding differ only slightly, the simplified formulation based on linearly polarized (LP) modes can be employed [45]

$$\frac{\left[\overline{J}_m(u) - \overline{Y}_m(u'\cdot\eta)\right]\left[\overline{K}_m(w) - \overline{J}_m(u')\right]}{\left[\overline{J}_m(u) - \overline{J}_m(u'\cdot\eta)\right]\left[\overline{K}_m(w) - \overline{Y}_m(u')\right]} = \frac{J_{m+1}(u'\cdot\eta)Y_{m+1}(u')}{J_{m+1}(u')Y_{m+1}(u'\cdot\eta)}, \tag{6}$$

where

$$u = a\sqrt{\kappa_0^2 n_1^2 - \beta^2}, \quad u' = b\sqrt{\kappa_0^2 n_2^2 - \beta^2}, \quad w = b\sqrt{\beta^2 - \kappa_0^2 n_3^2}, \tag{7}$$

are modal parameters; (a) and (b) are the radii of the core and cladding, respectively; ($\kappa_0 = 2\pi/\lambda$) is the free-space wavenumber; (η) is the core-to-cladding radius ratio; and (m) is the azimuthal mode order of the (LP_{mn}) mode. The quantities denoted with an overbar are calculated as:

$$\overline{V}_m(x) = \frac{V_m(x)}{x\cdot V_{m+1}(x)}, \tag{8}$$

where the function $V_m(x)$ corresponds to one of the cylindrical Bessel functions: the first kind $J_m(x)$, second kind $Y_m(x)$ (Neumann), or the modified Bessel functions $I_m(x)$ (Infeld) and $K_m(x)$ (Macdonald).

The calculation of the effective refractive index of the etched section is a key component of the model, since the etching depth directly controls the sensitivity of the structure. An external perturbation modifies the refractive index of the surrounding medium, which, through the modal field distribution, alters the effective refractive index in the localized segment. This perturbation is subsequently manifested as a change in the overall spectral response of the structure.

The present modal analysis is restricted to partially etched configurations that retain a residual cladding layer around the fiber core. Within this range, the fundamental guided mode remains predominantly localized in the core and residual-cladding regions, and the LP01 approximation is used as a reduced-order model for evaluating the dependence of the effective refractive index on the external medium. The model is not intended to describe nearly fully uncladded fibers or high-contrast external-media conditions in which a substantial fraction of the modal field reaches the outer boundary. Such cases require a full-vector electromagnetic analysis and are outside the scope of the present concept study.

In the present model, the etching depth is characterized by the residual cladding radius b (or equivalently the residual cladding diameter $D_{CL} = 2b$). The influence of the etching depth was evaluated in [49], where the residual cladding diameter was varied from 125 µm (unetched fiber) down to 12 µm. The research established that decreasing the residual cladding diameter increases the interaction of the guided mode with the external medium and consequently enhances the refractive-index sensitivity. A pronounced increase in sensitivity is observed when D_{CL} becomes smaller than approximately 13–15 µm. However, a strongly nonlinear response emerges as the residual cladding approaches the core radius ($D_{CL} < 12$ µm), restricting the usable linear sensing range. In the current work, the cladding diameter D_{CL} is set to be equal to 13 µm to ensure both sufficient sensitivity and linearity of the response.

3.3. Model Assumptions and Validity Conditions

The model is based on several physical and geometrical assumptions. First, it is assumed that light propagation in the structure can be described in terms of the fundamental guided mode, and the effective refractive index of the etched segment is primarily associated with the fundamental LP_{01} mode. Second, each homogeneous FBG is described within a one-dimensional transfer matrix framework as a periodic structure with segment-wise constant parameters, including its length, period, induced refractive index modulation, and effective refractive index. Third, the intermediate sections between the FBG segments are treated as uniform fiber segments without any additional refractive index modulation.

In addition, the guided-mode condition must be satisfied, i.e., the fundamental mode must remain confined within the fiber core. This requirement imposes constraints on the admissible parameter space and is particularly important for structures with an etched cladding, since the model is only valid when the refractive index of the surrounding medium remains lower than that of the fiber core.

In terms of parameters, the model includes the optical wavelength (λ), the lengths of the three FBG segments (L), the lengths of the intermediate sections between them (S), the grating periods (Λ), the induced refractive index modulation (Δn), the effective refractive indices of each segment (n_{eff}), the core radius (a), the parameters of the residual cladding (b), and the refractive index of the surrounding medium (n_3). The refractive index of the fiber core, the induced refractive index modulation of the FBG, and the effective refractive index are all temperature-dependent through the thermo-optic coefficient [49]. For the etched segment, the effective refractive index becomes the key variable parameter, determined by both the etching geometry and the properties of the surrounding medium.

Thus, the theoretical framework integrates three levels of description: (i) a transfer-matrix model of the transmission spectrum of the addressed structure [50], (ii) a modal model of the etched segment with evaluation of the effective refractive index, and (iii) a set of physical constraints ensuring the validity of the guided-wave regime. This formulation enables the same model to be used both for designing the spectral response of the EAFBS and for subsequent analysis of the effects of the surrounding medium, temperature, and pH on the sensor's address frequency.

3.4. pH-to-Refractive-Index Calibration Model

For the numerical analysis, the influence of pH on the optical response of the EAFBS was introduced through a calibrated relationship between the pH value of the surrounding alkaline medium and its refractive index n_3 [51]. Since the refractive-index–pH relationship depends on the chemical composition, ionic strength, and temperature of the solution, a universal analytical expression does not exist. Therefore, a phenomenological calibration model was adopted for the considered media.

The refractive index of the surrounding medium was expressed as

$$n_3(pH) = n_{3,0} + K_{RI-pH}\,(pH - pH_0) + O\Big[(pH - pH_0)^2\Big].$$

where n_3 is the reference refractive index, pH_0 is the reference pH value, and K_{RI-pH} is the calibration coefficient describing the refractive-index variation with pH. The last term represents the higher-order contributions to the refractive-index variation with pH, including the local nonlinear component of the calibration dependence. Its magnitude is proportional to, or smaller than, the square of the deviation $(pH - pH_0)^2$; therefore, it is neglected within the first-order approximation over a sufficiently narrow pH interval.

To account for the dependence of the refractive-index response on the composition of the liquid medium, the calibration coefficient K_{RI-pH} was assigned different values for different application domains. In the pH range 4.7–7.0, corresponding to water-quality monitoring applications [52], the coefficient is denoted as K_1. In the pH range 7.0–10.0, corresponding to neutral and mildly alkaline microbial culture and bioprocessing media [53], the coefficient is denoted as K_2. In the pH range 10.0–13.0, corresponding to strongly alkaline aqueous solutions [54], the coefficient is denoted as K_3.

This calibration model was adopted to emulate the refractive-index variations expected in alkaline aqueous media and is consistent with experimentally reported refractive-index behavior of NaOH solutions [55].

Changes in pH first modify the refractive index of the surrounding medium. These variations alter the effective refractive index of the etched segment, leading to a spectral shift in the transparency window and, consequently, to a change in the microwave-photonic address frequency.

4. Results

4.1. Variation in pH

The key output parameter of the proposed sensor is the address frequency, as it exhibits the most pronounced and robust dependence on variations in the pH of the surrounding medium. The simulation of the EAFBS spectral response was performed for three pH ranges with different calibration coefficients K_{RI-pH} mentioned above.

As the pH of the surrounding medium increases, the effective refractive index in the etched segment decreases, causing the left peak of the transmission window to shift progressively toward shorter wavelengths. At the same time, the address frequency varies nearly linearly in all the considered pH ranges. Thus, in the pH range from 4 to 7 it shifts from approximately 15 to 20 GHz, corresponding to a sensitivity of about 1.66 GHz/pH (Figure 4). The highest sensitivity of about 2.64 GHz/pH is demonstrated in the pH range from 7 to 10 due to the highest contribution of the applied calibration coefficient K_{RI-pH} (Figure 5), while in the range of pH 10–13, the sensitivity slightly decreased to 1.92 GHz/pH (Figure 6).

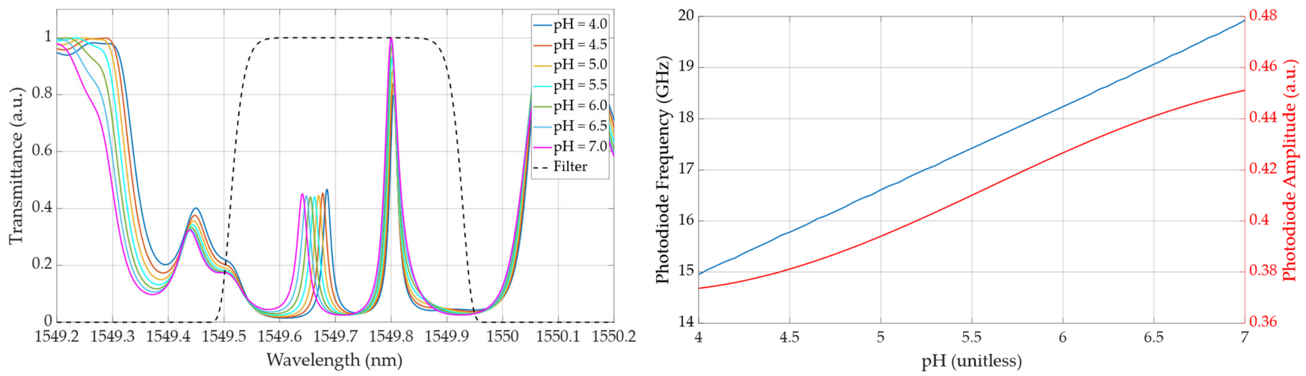

(**a**) (**b**)

Figure 4. Variation in the EAFBS transmission spectrum (**a**) and photodetector output signal (**b**) (address frequency—blue line, left axis; output current amplitude—red line, right axis) over the pH range of 4–7 with the address frequency sensitivity of 1.66 GHz/pH.

Concurrently, the amplitude of the photodetector output current at the address frequency also changes with increasing pH (Figures 4b, 5b and 6b, red curve).

The amplitude response generally exhibits a nonlinear behavior, with a maximum variation of approximately 7–22% per unit pH relative to its current value. This enables the amplitude channel to be used as an auxiliary output parameter to enhance measurement robustness or to implement a dual-parameter calibration scheme. However, in the basic configuration, the address frequency can be considered the primary measurement parameter, as its dependence on pH is more readily interpretable and metrologically more stable.

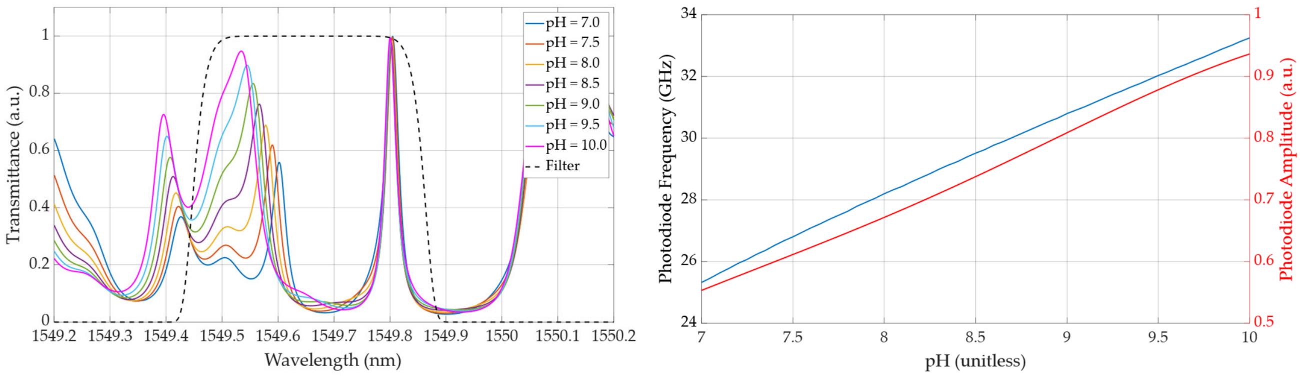

(**a**) (**b**)

Figure 5. Variation in the EAFBS transmission spectrum (**a**) and photodetector output signal (**b**) (address frequency—blue line, left axis; output current amplitude—red line, right axis) over the pH range of 7–10 with the address frequency sensitivity of 2.64 GHz/pH.

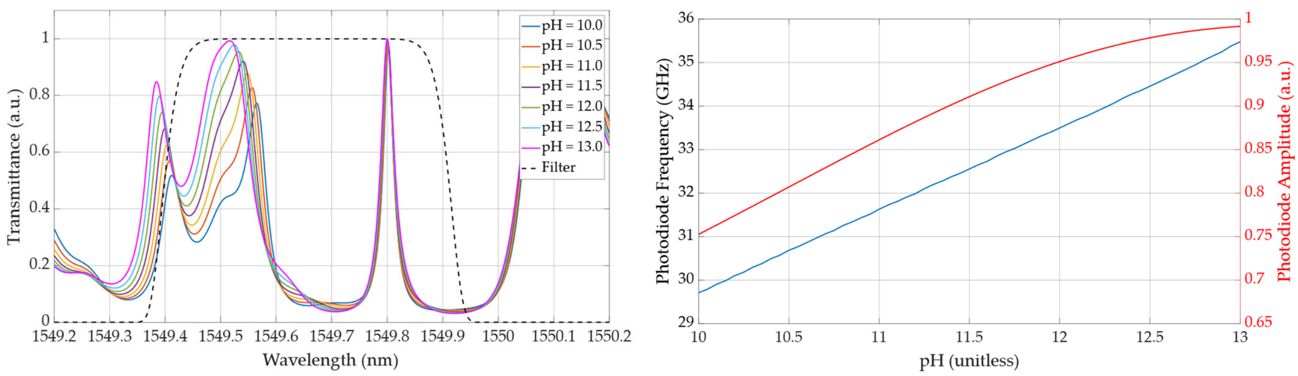

(**a**) (**b**)

Figure 6. Variation in the EAFBS transmission spectrum (**a**) and photodetector output signal (**b**) (address frequency—blue line, left axis; output current amplitude—red line, right axis) over the pH range of 10–13 with the address frequency sensitivity of 1.92 GHz/pH.

Since pH is the primary measurand in the proposed sensing approach, it is also necessary to evaluate the influence of temperature variations on the sensor response. Although the sensing mechanism is based on pH-induced changes in the refractive index of the surrounding medium, temperature fluctuations may affect the spectral characteristics of the structure and introduce measurement uncertainty. Therefore, the temperature response was analyzed separately to assess the temperature cross-sensitivity of the proposed sensor.

4.2. Temperature Variation

Temperature cross-sensitivity is of critical importance for assessing the applicability of the sensor. Considering a thermo-optic coefficient of the studied medium to be equal to -1.12×10^{-4} as an example [56], temperature dependences of the EAFBS spectrum and photodetector output were studied. A temperature variation in the range from 35 °C to 45 °C leads to a shift in the EAFBS transmission spectrum toward longer wavelengths (Figure 7a).

In this case, the address frequency changes approximately linearly as well, with a coefficient of about 1.06 GHz/°C (Figure 7b). The amplitude of the photodetector output current at the address frequency exhibits a slight monotonic increase, with a maximum change not exceeding approximately 6.7% per °C. Overall, this indicates that the influence of temperature on the addressed response must be taken into account within the considered range by utilizing a temperature compensation approach based on the introduction of a separate temperature sensor, for instance.

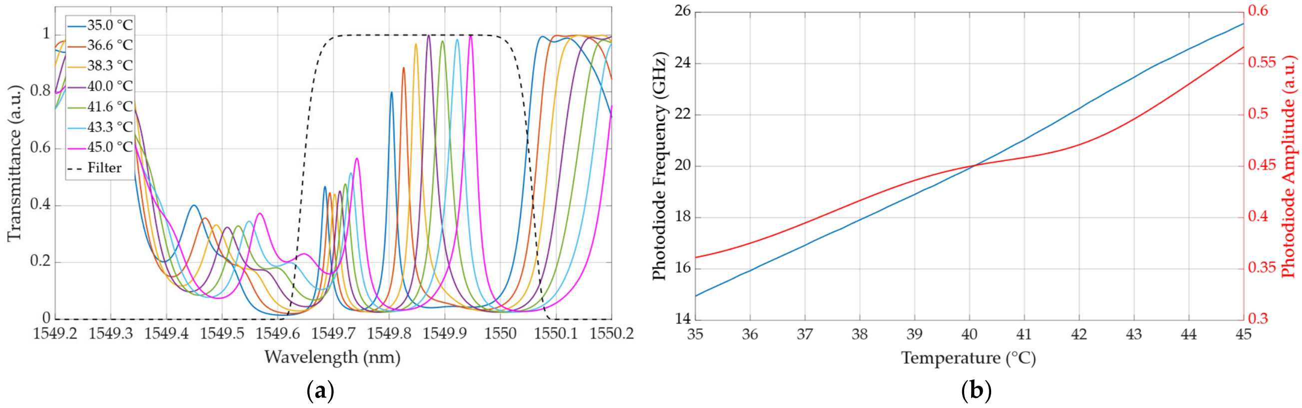

Figure 7. Variation in the EAFBS transmission spectrum over the temperature range 35–45 °C with sensitivity 0.017 GHz/°C (**a**) and photodetector output signal (**b**) (address frequency—blue line, left axis; output current amplitude—red line, right axis).

According to the present modeling results, in the operating ranges of pH from 4 to 7, from 7 to 10, and from 10 to 13, at temperatures of approximately 35−45 °C, a combination of three key properties is achieved: a monotonic dependence of the address frequency on pH, relatively low temperature cross-sensitivity, and high frequency sensitivity sufficient for precise measurements. The pH resolution can be estimated from the ratio between the frequency resolution of the interrogation system and the address-frequency sensitivity. For the calculated sensitivity of 1.66 GHz/pH in the pH range from 4 to 7, and assuming a practical frequency resolution of about 100 MHz, the estimated pH resolution is approximately:

$$\Delta pH = \frac{\Delta f}{S_{\text{pH}}} = \frac{100\ \text{MHz}}{1.66\ \text{GHz/pH}} \simeq 0.06$$

corresponding to an achievable resolution of approximately ±0.06 pH under the assumed interrogation conditions. For the other considered pH ranges, the estimated resolution is as follows: ±0.038 pH (pH 7–10) and ±0.052 pH (pH 10–13).

This behavior provides the physical basis for pH estimation via microwave-photonic interrogation of the address frequency.

5. Discussion

Due to the highly linear response of the address frequency to the pH of the surrounding medium, the frequency channel is the preferred option for practical implementation of the pH sensor, while the amplitude channel can be used as an auxiliary parameter for calibration or for enhancing measurement robustness.

Unlike conventional wavelength-tracking interrogation schemes that typically require high-resolution optical spectrum analyzers and complex spectral processing, the proposed EAFBS-based microwave-photonic approach transfers sensing information into the microwave-frequency domain through the address frequency. This enables simplified interrogation architecture, improved compatibility with high-speed electronic processing, and potential scalability for multiplexed sensing systems. In addition, frequency-domain interrogation may reduce the computational burden associated with continuous optical spectrum analysis, making the proposed approach attractive for distributed and real-time sensing applications.

The operating range of the sensor is determined by several factors. First, it is constrained by waveguiding conditions, as the refractive index of the surrounding medium must not exceed that of the fiber core. Second, it depends on the cladding etching depth: deeper etching increases sensitivity and extends the quasi-linear response region, but at the same time complicates fabrication and reduces the mechanical strength of the sensing element. Third, the conversion from refractive index to pH is not universal and requires calibration for a specific class of solutions. Therefore, the proposed structure should be regarded not as a universal pH sensor, but as a tunable sensing architecture tailored to a given class of liquid media.

Relatively high temperature cross-sensitivity of the EAFBS (~1 GHz/°C in aqueous solutions) requires a temperature compensation technique to be implemented in practical applications. One of the possible approaches in this regard can be the usage of a separate temperature sensor, which can be based on a non-etched addressed fiber Bragg structure with different address frequency utilizing the same interrogation setup. Alternatively, for a given medium under study with the known pH calibration coefficient, the data obtained during a series of calibration procedures at various temperatures can be used to retrieve the values of both pH and temperature using two sensors with different etching depths due to various responses of the frequency and amplitude channels to the measured parameters.

Another practical consideration is the chemical stability of the etched silica region in strongly alkaline environments. At elevated pH values, prolonged exposure may lead to gradual modification of the silica surface and changes in the sensor characteristics over time. In practical implementations, this issue may be addressed through optimization of the operating conditions, limitation of exposure duration, or the use of protective functional coatings compatible with refractive-index sensing. A detailed experimental investigation of long-term chemical stability is beyond the scope of the present theoretical study and will be addressed in future work.

Overall, the EAFBS concept appears most promising as a specialized sensing platform in which the sensing element, optical filtering, and microwave-frequency signal processing are co-designed. For stable operation, the spectral response of the EAFBS must be matched to the optical bandpass filter and photodetector so that only the high-Q spectral components forming the address frequency contribute to digital signal processing. This approach is particularly justified in applications where high data acquisition speed and a simplified interrogation scheme are critical. Additional challenges may be associated with the need for individual calibration for specific media and with limitations imposed by the waveguiding nature of the structure.

Several practical aspects remain to be investigated in future studies. In particular, experimental validation of the proposed EAFBS architecture will be necessary to confirm the theoretically predicted spectral behavior and address-frequency response under realistic operating conditions. Future work will also focus on optimization of the microwave-photonic interrogation unit, investigation of fabrication tolerances and structural asymmetries, and evaluation of noise-related effects, including laser instability, photodetector nonlinearities, and ADC quantization limitations.

Further work should focus on the experimental fabrication and validation of the proposed EAFBS sensing architecture under realistic operating conditions, including investigation of the combined influence of pH and temperature variations, coupled thermo-mechanical-chemical effects, fabrication tolerances, and long-term stability of the etched sensing region. The implementation of multiplexed configurations for distributed multi-parameter monitoring should also be investigated. Since the present results are based exclusively on theoretical analysis and numerical simulations, these studies will be necessary to assess the robustness, repeatability, and practical applicability of the proposed concept and to support its transition from a theoretical model to high-speed microwave-photonic sensing systems.

6. Conclusions

Theoretical analysis demonstrates that a modified addressed fiber Bragg structure with an etched cladding segment can serve as the sensing element of a microwave-photonic system for local pH monitoring. In this work, we provisionally divide the simulated pH values into three ranges with various calibration coefficients, thereby illustrating the applicability of the proposed sensing element for various media under study. It is shown that, in the three considered pH ranges covering values from 4 to 13, the address frequency varies nearly linearly in each of the ranges with a sensitivity of 1.66–2.64 GHz/pH, while its temperature dependence in the range of 35–45 °C is approximately 1 GHz/°C. This supports the use of the address frequency as the primary measurement parameter for microwave-photonic interrogation.

At the same time, the proposed approach is not a universal pH measurement method, as it requires calibration for a specific class of media and adherence to constraints associated with the waveguiding regime and the geometry of the etched segment. Overall, the EAFBS concept represents a promising specialized platform for high-speed pH monitoring in applications where a simple interrogation scheme, frequency-domain operation, and the potential for extension to multiplexed configurations are critical.

The proposed architecture extends the applicability of addressed fiber Bragg structures toward microwave-photonic sensing systems in which the measured information is encoded in the frequency domain through transformations of the addressed spectral response. The presented approach demonstrates the potential of EAFBS-based microwave-photonic interrogation for high-speed sensing applications and future multiplexed photonic sensor networks.

Author Contributions: Conceptualization, A.N.D.A. and A.Z.S.; methodology, T.A.A.; software, B.I.V.; validation, A.A.K. (Aliya A. Kamaleeva) and A.N.D.A.; formal analysis, A.Z.S.; investigation, A.N.D.A., B.I.V. and A.A.K. (Aliya A. Kamaleeva); data curation, B.I.V., T.A.A. and A.Z.S.; writing—original draft preparation, A.N.D.A. and A.Z.S.; writing—review and editing, B.I.V., T.A.A. and A.Z.S.; visualization, B.I.V. and A.A.K. (Artem A. Kuznetsov); supervision, A.A.K. (Artem A. Kuznetsov); project administration, A.A.K. (Artem A. Kuznetsov); funding acquisition, A.A.K. (Artem A. Kuznetsov). All authors have read and agreed to the published version of the manuscript.

Funding: The work was carried out within the framework of the state assignment FZSU-2026-0009 (Reg. No NIOKTR 126020516512-7).

Data Availability Statement: The data supporting the findings of this study are available from the corresponding author upon reasonable request.

Conflicts of Interest: The authors declare no conflicts of interest.

References

1. Becskereki, G.; Horvai, G.; Tóth, B. Adsorption of Hydrophobic Ions on Environmentally Relevant Sorbents. *Polymers* **2022**, *14*, 3167. [CrossRef] [PubMed]
2. Gibson, M.; Newsham, P. Acids and Bases. In *Food Science and the Culinary Arts*; Elsevier: Amsterdam, The Netherlands, 2018; pp. 105–109, ISBN 978-0-12-811816-0.
3. Swindlehurst, B.R.; Narayanaswamy, R. Optical Sensing of pH in Low Ionic Strength Waters. In *Optical Sensors*; Springer Series on Chemical Sensors and Biosensors; Springer: Berlin/Heidelberg, Germany, 2004; Volume 1, pp. 281–308, ISBN 978-3-642-07421-9.
4. Nazaroff, W.W.; Weschler, C.J. Indoor Acids and Bases. *Indoor Air* **2020**, *30*, 559–644. [CrossRef] [PubMed]
5. Agmon, N.; Bakker, H.J.; Campen, R.K.; Henchman, R.H.; Pohl, P.; Roke, S.; Thämer, M.; Hassanali, A. Protons and Hydroxide Ions in Aqueous Systems. *Chem. Rev.* **2016**, *116*, 7642–7672. [CrossRef] [PubMed]

6. Morozov, O.; Tunakova, Y.; Hussein, S.M.R.H.; Shagidullin, A.; Agliullin, T.; Kuznetsov, A.; Valeev, B.; Lipatnikov, K.; Anfinogentov, V.; Sakhabutdinov, A. Addressed Combined Fiber-Optic Sensors as Key Element of Multisensor Greenhouse Gas Monitoring Systems. *Sensors* **2022**, *22*, 4827. [CrossRef] [PubMed]
7. Villasana, Y.; Moradi, N.; Navas-Cárdenas, C.; Patience, G.S. Experimental Methods in Chemical Engineering: pH. *Can. J. Chem. Eng.* **2022**, *100*, 1703–1717. [CrossRef]
8. Akhtar, M.H.; Nawaz, M.A.H.; Abbas, M.; Liu, N.; Han, W.; Lv, Y.; Yu, C. Advances in pH Sensing: From Traditional Approaches to Next-Generation Sensors in Biological Contexts. *Chem. Rec.* **2024**, *24*, e202300369. [CrossRef] [PubMed]
9. Frankær, C.G.; Hussain, K.J.; Dörge, T.C.; Sørensen, T.J. Optical Chemical Sensor Using Intensity Ratiometric Fluorescence Signals for Fast and Reliable pH Determination. *ACS Sens.* **2019**, *4*, 26–31. [CrossRef] [PubMed]
10. Liu, T.; Wang, W.; Ding, H.; Yi, D. Smartphone-Based Hand-Held Optical Fiber Fluorescence Sensor for On-Site pH Detection. *IEEE Sens. J.* **2019**, *19*, 9441–9446. [CrossRef]
11. Rosenberg, M.; Laursen, B.W.; Frankær, C.G.; Sørensen, T.J. A Fluorescence Intensity Ratiometric Fiber Optics–Based Chemical Sensor for Monitoring pH. *Adv. Mater. Technol.* **2018**, *3*, 1800205. [CrossRef]
12. Chen, W.-H.; Dillon, W.D.N.; Armstrong, E.A.; Moratti, S.C.; McGraw, C.M. Self-Referencing Optical Fiber pH Sensor for Marine Microenvironments. *Talanta* **2021**, *225*, 121969. [CrossRef] [PubMed]
13. Chauhan, M.; Singh, V.K. Fiber Optic pH Sensor Using TiO2-SiO2 Composite Layer with a Temperature Cross-Sensitivity Feature. *Optik* **2020**, *212*, 164709. [CrossRef]
14. Bhardwaj, V.; Pathak, A.K.; Singh, V.K. No-Core Fiber-Based Highly Sensitive Optical Fiber pH Sensor. *J. Biomed. Opt.* **2017**, *22*, 057001. [CrossRef] [PubMed]
15. Huang, Y.; Wang, E.-B.; Li, P.; Cao, J.-W.; Lyu, G.-H. pH Sensor Based on Tilted Fiber Bragg Grating Surface Plasmon Resonance with a Polyaniline Reaction Deposition Film Layer. *Opt. Express* **2024**, *32*, 10887. [CrossRef] [PubMed]
16. Li, L.; Zhang, Y.-N. Fiber-Optic SPR pH Sensor Based on MMF–NCF–MMF Structure and Self-Assembled Nanofilm. *IEEE Trans. Instrum. Meas.* **2021**, *70*, 9502509. [CrossRef]
17. Puppulin, L.; Hosogi, S.; Sun, H.; Matsuo, K.; Inui, T.; Kumamoto, Y.; Suzaki, T.; Tanaka, H.; Marunaka, Y. Bioconjugation Strategy for Cell Surface Labelling with Gold Nanostructures Designed for Highly Localized pH Measurement. *Nat. Commun.* **2018**, *9*, 5278. [CrossRef] [PubMed]
18. Engholm, M.; Hammarling, K.; Andersson, H.; Sandberg, M.; Nilsson, H.-E. A Bio-Compatible Fiber Optic pH Sensor Based on a Thin Core Interferometric Technique. *Photonics* **2019**, *6*, 11. [CrossRef]
19. Yi, X.; Zhao, K.; Chen, K.P. Multiplexable Fiber pH Sensors Enabled by Intrinsic Fabry-Perot Interferometer Array. *IEEE Sens. J.* **2022**, *22*, 2167–2171. [CrossRef]
20. Wang, Y.R.; Tou, Z.Q.; Ravikumar, R.; Lim, Y.Y.; Ding, Z.W.; Zhao, C.L.; So, P.L.; Chan, C.C. Reflection-Based Thin-Core Modal Interferometry Optical Fiber Functionalized With PAA-PBA/PVA for Glucose Detection Under Physiological pH. *J. Light. Technol.* **2019**, *37*, 2773–2777. [CrossRef]
21. Ran, Y.; Xiao, P.; Zhang, Y.; Hu, D.; Xu, Z.; Liang, L.; Guan, B.-O. A Miniature pH Probe Using Functional Microfiber Bragg Grating. *Optics* **2020**, *1*, 202–212. [CrossRef]
22. Saha, N.; Brunetti, G.; Armenise, M.N.; Ciminelli, C. A Compact, Highly Sensitive pH Sensor Based on Polymer Waveguide Bragg Grating. *IEEE Photonics J.* **2023**, *15*, 2200607. [CrossRef]
23. Li, P.; Huang, Y.; Wang, E.; Cao, J.; Pei, Y.; Lyu, G. Tilted Fiber Bragg Grating pH Sensor Based on Polyaniline Reaction Deposition Film Layer. *Opt. Quantum Electron.* **2024**, *56*, 1353. [CrossRef]
24. Urriza-Arsuaga, I.; Ielasi, G.; Bedoya, M.; Orellana, G. Luminescence-Based Sensors for Bioprocess Applications. In *Fluorescence in Industry*; Pedras, B., Ed.; Springer Series on Fluorescence; Springer International Publishing: Cham, Switzerland, 2019; Volume 18, pp. 1–38, ISBN 978-3-030-20032-9.
25. Chen, Z.; Meng, X.; Xie, M.; Shi, Y.; Zou, L.; Guo, S.; Jiang, J.; Liu, S.; Zhao, Q. A Self-Calibrating Phosphorescent Polymeric Probe for Measuring pH Fluctuations in Subcellular Organelles and the Zebrafish Digestive Tract. *J. Mater. Chem. C* **2020**, *8*, 2265–2271. [CrossRef]
26. Xiong, Y.; Huang, Y.; Ye, Z.; Guan, Y. Flow Injection Small-Volume Fiber-Optic pH Sensor Based on Evanescent Wave Excitation and Fluorescence Determination. *J. Fluoresc.* **2011**, *21*, 1137–1142. [CrossRef] [PubMed]
27. Li, H.; Wang, X.; Li, X.; Yu, H.-Z. Quantitative pH Determination Based on the Dominant Wavelength Analysis of Commercial Test Strips. *Anal. Chem.* **2021**, *93*, 15452–15458. [CrossRef] [PubMed]
28. Mahdi, K.A.S.; Al-Tahar, I.A.; Neamah, W.A.; Shakir, W.M.R. Realization of the Importance of Using Fiber Optic Sensor Technology in Engineering and Medical Applications: A Review. In Proceedings of the AIP Conference Proceedings, Baghdad, Iraq, 17 April 2024; Volume 3232, p. 040034.
29. Roriz, P.; Silva, S.; Frazão, O.; Novais, S. Optical Fiber Temperature Sensors and Their Biomedical Applications. *Sensors* **2020**, *20*, 2113. [CrossRef] [PubMed]

30. Huang, J.; Liu, T.; Zhang, Y.; Zhan, C.; Xie, X.; Yu, Q.; Yi, D. Smartphone-Based Optical Fiber Fluorescence Temperature Sensor. *Sensors* **2022**, *22*, 9605. [CrossRef] [PubMed]
31. Yang, H.; Shin, S.; Kumar, S.; Seo, D.; Oh, S.; Lee, M.; Seo, S. A CMOS Image Sensor Based Refractometer without Spectrometry. *Sensors* **2022**, *22*, 1209. [CrossRef] [PubMed]
32. Gambino, F.; Cicatiello, P.; Giaquinto, M.; Micco, A.; Aliberti, A.; Cusano, A.M.; Ricciardi, A.; Cusano, A. Cavity Enhanced Lab-on-Fiber Optrode for Ultra-Sensitive pH Monitoring. *Sens. Diagn.* **2022**, *1*, 534–540. [CrossRef]
33. Lopes, G.; Cennamo, N.; Zeni, L.; Singh, R.; Kumar, S.; Fernandes, A.J.S.; Costa, F.; Pereira, S.O.; Marques, C. Innovative Optical pH Sensors for the Aquaculture Sector: Comprehensive Characterization of a Cost-Effective Solution. *Opt. Laser Technol.* **2024**, *171*, 110355. [CrossRef]
34. Raoufi, N.; Surre, F.; Rajarajan, M.; Sun, T.; Grattan, K.T.V. Fiber Optic pH Sensor Using Optimized Layer-by-Layer Coating Approach. *IEEE Sens. J.* **2014**, *14*, 47–54. [CrossRef]
35. Liu, T.; Li, Y.; Dai, X.; Gan, W.; Wang, X.; Dai, S.; Song, B.; Xu, T.; Zhang, P. Simultaneous Detection of Temperature, Strain, Refractive Index, and pH Based on a Phase-Shifted Long-Period Fiber Grating. *J. Light. Technol.* **2023**, *41*, 5169–5180. [CrossRef]
36. Xiao, Y.; Wang, Y.; Zhu, D.; Shi, J.; Liu, Q.; Gao, L. Microwave-Photonic Optical Fiber Interferometers for Wavelength Interrogation of Fiber Bragg Grating Sensors with High Sensitivity and a Tunable Dynamic Range. *Appl. Opt.* **2023**, *62*, E32. [CrossRef] [PubMed]
37. Nordmeyer, U.; Thiel, T.; Kojucharow, K.; Neumann, N. On the Advantages of Microwave Photonic Interrogation of Fiber-Based Sensors: A Noise Analysis. *Sensors* **2023**, *23*, 3746. [CrossRef] [PubMed]
38. Morozov, O.G.; Sakhabutdinov, A.J. Addressed fiber Bragg structures in quasi-distributed microwave-photonic sensor systems. *Comput. Opt.* **2019**, *43*, 535–543. [CrossRef]
39. Misbakhov, R.S.; Vasev, A.N.; Sakhabutdinov, A.Z.; Nureev, I.I.; Morozov, O.G.; Lipatnikov, K.A.; Vasilets, A.A. Address Fiber Optical Sensor for Relative Humidity Measuring in a Switchgear. In *Proceedings of the SPIE International Society for Optical Engineering*; Andreev, V.A., Bourdine, A.V., Burdin, V.A., Morozov, O.G., Sultanov, A.H., Eds.; SPIE: Washington, DC, USA, 2020; Volume 11516.
40. Agliullin, T.A.; Gubaidullin, R.R.; Ivanov, V.; Morozov, O.G.; Sakhabutdinov, A.Z. Addressed FBG-Structures for Tire Strain Measurement. In *Proceedings of the XVI International Scientific and Technical Conference on Optical Technologies in Telecommunications 2018, Ufa, Russia, 20–22 November 2018*; Andreev, V.A., Bourdine, A.V., Burdin, V.A., Morozov, O.G., Sultanov, A.H., Eds.; SPIE: Washington, DC, USA, 2019; Volume 11146, p. 6.
41. Agliullin, T.; Gubaidullin, R.; Sakhabutdinov, A.; Morozov, O.; Kuznetsov, A.; Ivanov, V. Addressed Fiber Bragg Structures in Load-Sensing Wheel Hub Bearings. *Sensors* **2020**, *20*, 6191. [CrossRef] [PubMed]
42. Kuznetsov, A.A.; Nureev, I.I.; Lipatnikov, K.A. Fiber Optic Sensors with Polarization Multiplexing Based on Addressed Fiber Bragg Gratings. In Proceedings of the 2020 Systems of Signals Generating and Processing in the Field of on Board Communications, Moscow, Russia, 19–20 March 2020; pp. 1–5.
43. Koo, K.P.; LeBlanc, M.; Tsai, T.E.; Vohra, S.T. Fiber-Chirped Grating Fabry-Perot Sensor with Multiple-Wavelength-Addressable Free-Spectral Ranges. *IEEE Photonics Technol. Lett.* **1998**, *10*, 1006–1008. [CrossRef]
44. Sun, Q.; Li, X.; Zhang, M.; Liu, Q.; Liu, H.; Liu, D. High Capacity Fiber Optic Sensor Networks Using Hybrid Multiplexing Techniques and Their Applications. In *Proceedings of the 2013 International Conference on Optical Instruments and Technology: Optical Sensors and Applications*; SPIE: Washington, DC, USA, 2013; Volume 9044, pp. 142–151.
45. Miao, Y.; Liu, B.; Zhang, H.; Li, Y.; Zhou, H.; Sun, H.; Zhang, W.; Zhao, Q. Relative Humidity Sensor Based on Tilted Fiber Bragg Grating with Polyvinyl Alcohol Coating. *IEEE Photonics Technol. Lett.* **2009**, *21*, 441–443. [CrossRef]
46. Zhu, C.; Alsalman, O.; Huang, J. Microwave-Photonic Vernier Effect Enabled High-Sensitivity Fiber Bragg Grating Sensors for Point-Wise and Quasi-Distributed Sensing. *Opt. Express* **2023**, *31*, 41996. [CrossRef] [PubMed]
47. Yang, Y.; Liu, J.; Zhou, X. A CRISPR-Based and Post-Amplification Coupled SARS-CoV-2 Detection with a Portable Evanescent Wave Biosensor. *Biosens. Bioelectron.* **2021**, *190*, 113418. [CrossRef] [PubMed]
48. Gaston, A.; Lozano, I.; Perez, F.; Auza, F.; Sevilla, J. Evanescent Wave Optical-Fiber Sensing (Temperature, Relative Humidity, and pH Sensors). *IEEE Sens. J.* **2003**, *3*, 806–811. [CrossRef]
49. Alhussein, A.N.D.; Qaid, M.R.T.M.; Agliullin, T.A.; Valeev, B.I.; Kuznetsov, A.A.; Fedotov, M.Y.; Morozov, O.G.; Sakhabutdinov, A.Z. Etched Addressed Fiber Bragg Structures for Environment pH Sensing. *Laser Phys.* **2025**, *35*, 096201. [CrossRef]
50. Agliullin, T.; Il'In, G.; Kuznetsov, A.; Misbakhov, R.; Misbakhov, R.; Morozov, G.; Morozov, O.; Nureev, I.; Sakhabutdinov, A. Overview of Addressed Fiber Bragg Structures' Development. *Photonics* **2023**, *10*, 175. [CrossRef]
51. Monerie, M. Propagation in Doubly Clad Single-Mode Fibers. *IEEE Trans. Microw. Theory Tech.* **1982**, *30*, 381–388. [CrossRef]
52. Ohodnicki, P.R.; Wang, C. Optical Waveguide Modeling of Refractive Index Mediated *p* H Responses in Silica Nanocomposite Thin Film Based Fiber Optic Sensors. *J. Appl. Phys.* **2016**, *119*, 064502. [CrossRef]
53. Hoang, V.T.; Stępniewski, G.; Czarnecka, K.H.; Kasztelanic, R.; Long, V.C.; Xuan, K.D.; Shao, L.; Śmietana, M.; Buczyński, R. Optical Properties of Buffers and Cell Culture Media for Optofluidic and Sensing Applications. *Appl. Sci.* **2019**, *9*, 1145. [CrossRef]

54. Hausmann, J.N.; Traynor, B.; Myers, R.J.; Driess, M.; Menezes, P.W. The pH of Aqueous NaOH/KOH Solutions: A Critical and Non-Trivial Parameter for Electrocatalysis. *ACS Energy Lett.* **2021**, *6*, 3567–3571. [CrossRef]
55. Galindo-Luna, Y.R.; Gómez-Arias, E.; Ibarra-Bahena, J.; Morales-Flores, A.; Romero, R.J. New Concentration Correlations of NaOH Aqueous Solutions for a Thermodynamic Process. *J. Chem. Eng. Data* **2019**, *64*, 5302–5311. [CrossRef]
56. Ruiz-Perez, V.I.; Velasco-Bolom, P.M.; May-Arrioja, D.A.; Sepúlveda, J.R.G. Measuring the Thermo-Optic Coefficient of Liquids with Athermal Multimode Interference Devices. *IEEE Sens. J.* **2021**, *21*, 3004–3012. [CrossRef]